Supplementary Information

Orthogonal Nanopores Cross-Validation for Multiplex Single-Molecule Profiling

Lin-Lin Zhang,[a] Fan Gao,[a] Yi-He Wei,[a] Cheng-Bing Zhong,[a]
Bingqing Xia,[b,c] Liuqing Wen,[c,d] Yi-Tao Long,[a] and Yi-Lun Ying*[a,e]

[a] *Molecular Sensing and Imaging Center, School of Chemistry, Nanjing University, Nanjing 210023 (P. R. China). E-mail: yilunying@nju.edu.cn*

[b] *School State Key Laboratory of Drug Research, Shanghai Institute of Materia Medica, Chinese Academy of Sciences, Shanghai 201203 (P. R. China).*

[c] *University of Chinese Academy of Sciences, Beijing 100049 (P. R. China).*

[d] *Carbohydrate-Based Drug Research Center, Shanghai Institute of Materia Medica, Chinese Academy of Sciences, Shanghai 201203 (P. R. China)*

[e] *Chemistry and Biomedicine Innovation Center, Nanjing University, Nanjing 210023 (P. R. China)*

Table of Contents

Materials and Methods

Reagents and Chemicals

Decane (anhydrous, ≥99%), potassium chloride (KCl, ≥ 99%), Tris(hydroxymethyl)aminomethane (Tris, ≥99%), and Trypsin-EDTA were purchased from Sigma-Aldrich Co., Ltd. (St. Louis, MO, USA). 1, 2- Diphytanoyl-sn-glycero-3-phosphocholine (DPhPC, ≥99%) was purchased from Avanti Polar Lipids Inc. (Alabaster, Al, USA). Hydrochloric acid (HCl, 36 wt%) was purchased from Nanjing Chemical Reagent Co., Ltd. (Nanjing, China). Isopropanol (≥99.5%) was purchased from Shanghai Aladdin Biochemical Technology Co., Ltd. (Shanghai, China). Chloroform (≥99.5%) and acetone (≥99.5%) was purchased from Sinopharm Chemical Reagent Co., Ltd. (Shanghai, China). Sodium hypochlorite bleach (NaOCl, available chlorine 34.0 g/L) was purchased from Jiangsu Aitefu Co., Ltd. (Huai'an, China). For the microfabrication, the SU-8 2010 photoresist and SU-8 developer (PGMEA) were purchased from Kayaku Advanced Materials, Inc. (Westborough, USA). The ROL-7133 resist and the developer zx-238 were purchased from Suzhou Research Materials Microtech Co., Ltd (Suzhou, China). The chromium, gold, silver (99.999%) used for evaporation were purchased from Kurt J. Lesker Company® (Jefferson Hills, USA). Commercial Ag/AgCl electrode with a diameter of 2 mm was purchased from Wuhan Brain Link Technology (Wuhan, China). The quartz (SiO_2) substrate was purchased from Donghai Yibo Quartz Products Co., Ltd. (Lianyungang, China). Silver nitrate ($AgNO_3$, ≥98%) was purchased from Shanghai Hushi Chemical Reagent & Analysis Instrument Co. Ltd. (Shanghai, China). Ammonia water ($NH_3 \cdot H_2O$) was purchased from Shanghai Macklin Biochemical Technology Co., Ltd. (Shanghai, China). Water-DEPC treated water was purchased from Sangon Biotech Co., Ltd. (Shanghai, China). Fetal Bovine Serum (FBS, 10099141C) was purchased from Thermo Fisher Scientific Inc. (Shanghai, China). Flavin Adenine Dinucleotide (FAD, 97%) was purchased from Meryer (Shanghai) Biochemical Technology Co., Ltd. (Shanghai, China).

Poly$(dA)_4$ (5'-AAAA-3', dA_4), wild-type (WT) Epidermal Growth Factor Receptor (EGFR) circulating tumor DNA (ctDNA) segment (5'-ATCAC-3'), T790M mutant of EGFR ctDNA segment (5'-ATCAT-3'), microRNA-21 (miR-21) segment (5'-UAGCUUAUC-3') and miR-92a segment (5'-UAUUGCAC-3') were synthesized and HPLC-purified by Sangon Biotech Co., Ltd. (Shanghai, China). Programmed Cell Death Ligand 1 (PD-L1) fragment (LQDAGVYR) and its phosphorylation (LQDAGVY_pR, p-PD-L1) were synthesized and HPLC-purified by GL Biochem (Shanghai) Ltd. (Shanghai, China). Polylactosamine (Galβ1-4GlcNAcβ1-3Galβ1-4GlcNAc, DiLacNAc), lacto-*N*-tetraose (Galβ1-3GlcNAcβ1-3Galβ1-4Glc, LNT) and lacto-*N*-neotetraose (Galβ1-4GlcNAcβ1-3Galβ1-4Glc, LNnT) were enzymatically synthesized by Liuqing Wen's Lab as previously reported.[1] Specially, LNT and LNnT were synthesized from Galβ1-4Glc-OR, while DiLacNAc was synthesized from GlcNAc-OR using glycosyltransferases.

The reagents and materials we used are all the analytical grade. All solutions were prepared using ultrapure water (18.2 MΩ cm at 25 °C) from a Milli-Qsystem (Billerica, MA, USA).

Multiplex nanopore microchip fabrication

The microchip features a three-layer structure is designed for multiplex biomolecule sensing, incorporating 24 channels partitioned into six groups within separated chambers (Fig. S1). As described in previous work,[2] the microchip was prepared through microfabrication (Fig. S2). Fabrication commenced by patterning the wire areas on a cleaned SiO_2 substrate using ROL-7133 photoresist via photolithography (SUSS MicroTec Solutions GmbH & Co. KG, Garching, Germany), followed by the electron beam evaporation (EBE) from Kurt J. Lesker Company® (Jefferson Hills, USA) of Cr (10 nm)/Au (150 nm) to establish connections to the amplifier array. Then ROL-7133 was used again to define electrode areas following by evaporating Ag (500 nm) on the Au layer. Subsequently, an insulating supporting layer was formed by patterning SU-8 2010 photoresist into a microwell array with 50 μm diameter. Specially, the $Ag/AgCl_{cis}$ electrodes were integrated onto the chip through an additional electrodeposition process. Adapt the 0.3 M $AgNO_3$ in 1 M $NH_3 \cdot H_2O$ for Ag layer electroplating using a three-electrode cell (the patterned Ag on the microchip as the working electrode, an Ag wire quasi-reference electrode, and a Pt wire counter electrode) at room temperature conducted by CHI 852D from Shanghai Chenhua Co., Ltd. (Shanghai, China) (Fig. S3). This plating was driven at 0.33 mA/mm^2 (475 μA per pattern, the size of each $Ag/AgCl_{cis}$ electrode is 1.8 mm × 0.8 mm) for 150 s to achieve a thickness of approximately 3 μm, enhancing electrode stability (Fig. 2a). Finally, the microchip was chlorinated by immersion in NaClO solution for 3 min to form the Ag/AgCl electrode, subsequently cleaned with ultrapure water, dried,

and sealed for storage. While the electrode potential exhibited instability after multiple uses, functionality was reliably restored through re-oxidation in NaClO solution (Fig. 2b). Upon the microchip, independent chambers were formed with the composition of circular holes and sealing rings for independent nanopore sensing.

Multiplex nanopore microchip characterization

The depths and profiles of microchip were measured by Step Profiler DektakXT from Bruker (Billerica, USA). The parameters were set with the range of 65.5 μm and force at 2 mg. When testing the microwell, the probe scans a 300 μm path for 10 s, starting from the supporting (SU-8) layer at the microwell edge, traversing the depression of the microelectrode with a diameter of 50 μm as $Ag/AgCl_{trans}$ electrode, and returning to the SU-8 layer. The measured height difference represents the depth from the electrode layer to the SU-8 layer. While for $Ag/AgCl_{cis}$ electrode measuring, a 2400 μm path is scanned for 12 s, starting from the SU-8 layer, traversing the depression of the $Ag/AgCl_{cis}$ electrode layer, and ending at the SU-8 layer on the opposite side. The difference between these two measured depths yields the thickness of the electroplated Ag layer (Fig. 2a). The depths of microwells and electrodes were tested in 3 chambers separately.

OCP measurements were performed on CHI 852D in 1 M Tris-KCl, 1 mM EDTA, pH 8.0 buffer solution at the sampling interval time of 0.1 s for 2 h. The OCP of 3 independent $Ag/AgCl_{trans}$ microelectrodes were measured for 2 h. The OCP of the firstly measured $Ag/AgCl_{cis1}$ electrode and its second round ($Ag/AgCl_{cis2}$) versus commercial Ag/AgCl electrode were tested respectively. The OCP between $Ag/AgCl_{trans}$ and $Ag/AgCl_{cis}$ electrode was tested as well (Fig. 2b).

Nanopore experiments

Proaerolysin for WT Aerolysin (AeL), K238Q (KQ) AeL, T232K/K238Q (TK/KQ) AeL nanopore, and WT Outer membrane protein F (OmpF) nanopore performed in our laboratory as described in published works.[1,3-5] Proaerolysin was activated by incubating with trypsin-EDTA at a mass ratio of 50:3 for 5 h at room temperature. First, connect the microchip with the homemade instrument within high bandwidth ultra-low-current amplifier array. Then, each chamber received 200 μL of buffer solution (1.0 M KCl, 10 mM Tris, pH 8.0). When detecting miRNA, DEPC-treated water was used as the solvent to minimize RNA degradation. A bilayer lipid membrane (BLM) array was formed using the air bubble method, that a 10 μL pipette tip was immersed in 30 mg/mL DPhPC in decane solution and gently squeezed to deposit an air bubble onto the microwell array, facilitating lipid membrane spreading. Pore-forming proteins were then added, and a positive voltage was applied across the membrane to enable nanopore assembly. Finally, analyte biomolecules dissolved in 10 mM Tris-HCl were introduced into the chambers and mixed via pipetting for multiplex biomolecule sensing. The voltage of +80 mV to +140 mV was applied for biomolecules detection with AeL nanopore, while -80 mV to -120 mV was applied in OmpF nanopore sensing (Fig. 3, Fig. S8-S10).

Current signals were recorded using the homemade multichannel ultra-low-current amplifier array and digital circuit, with data recorded by dedicated software. Each channel in one chamber was independently connected to the amplifier array through spring-plunger-contacted Au pads, enabling stable and parallel recordings. The amplification instrument was fabricated using a mature and low-cost printed circuit board (PCB), providing good scalability and cost-effectiveness for multiplex nanopore sensing. For automitic operation, the liquid handling system from PRCXI Bioinformatics Co., Ltd. (Suzhou, China) were used to pipette solution and analyte, as well as the air bubbles automically pipetted to spread membrane array across all channels in each chamber (Fig. S23). Briefly, the microchip was aligned with the pipette array of the liquid handling workstation, followed by automated buffer loading into each chamber. Lipid bilayer membrane arrays were then formed through pipetting the lipid solution onto the microwell array to generate an air bubble for lipid spreading, followed by controlled air-bubble removal to produce bilayer membranes. Membrane quality was monitored through membrane voltage and capacitance measurements, and unstable membranes could be automatically re-formed through repeated air bubble pipetting cycles. After bilayer formation, different nanopores and analyte samples were sequentially added into individual chambers for parallel measurements. For comparison, single-channel nanopore sensing was performed using the homemade

Cube-D0 instrument and a thin-film chamber with a 50 μm aperture (Fig. S6).[6,7] All data was sampled at 100 kHz and filtered at 5 kHz. Nanopore experiments were conducted at 24 ± 2 °C.

Data processing

All the current data were analyzed with MOSAIC 1.3 software.[8] For data processing, the baseline was defined as the mean open-pore current (I_0), with the event threshold set to 5 times the baseline's standard deviation (STD). The scatter plots could be divided into translocation events and collision events, according to the previous study[9]. Collision and distorted events with the duration time (t) < 0.16 ms as well as residual current depth (I/I_0) shorted than 0 and I/I_0 large than 0.9 were excluded during machine learning preprocessing. Current traces were visualized using Clampfit 10.2 (Molecular Devices LLC, San Jose, CA, USA), while analyzed results were plotted in OriginPro (OriginLab Corporation, Northampton, MA, USA). The extracted blockades were analyzed statistically by using Gaussian fittings to the histogram of the I/I_0. The duration time was calculated with Gaussian fitting to the histogram of logarithmically transformed blockage time. The capture frequency (f) of the blockades was calculated by $f = 1/\tau_{on}$, where τ_{on} represents the interval time. Only the signals corresponding to the I/I_0 peak were included in the calculation, while the surrounding scattered points were excluded. The τ_{on} was analyzed statistically by using Gaussian fitting to the histogram of the logarithm.

Machine learning and linear fitting model

To enable molecular classification and concentration prediction, we employed ML models trained on data acquired from four distinct nanopores: WT AeL, KQ AeL, TK/KQ AeL, and WT OmpF. Each nanopore was used to detect multiple biomolecules: Poly(dA)$_4$, WT EGFR, miR-21, PD-L1, DiLacNAc, and FAD. This setup allowed each nanopore-specific ML model to classify events from any of the above analytes.

Firstly, pure analyte datasets (500-2000 events per analyte per nanopore) were generated and input into the model. Each event was characterized by two features extracted via MOSAIC software: I/I_0, Log(t). To address inherent nanopore background noise, we applied the Hierarchical Density-Based Spatial Clustering of Applications with Noise (HDBSCAN)[1,10] algorithm as a pretreatment step. Parameters were set to *neighborhood size* = 0.15, and *min samples* = 5 for AeL and *min samples* = 2 for OmpF, due to the OmpF showed less background signals. This effectively filtered out events unable to form distinct clusters, preserving the primary distribution characteristics of each analyte. Analytes yielding fewer than 10 events after HDBSCAN were treated as unclassifiable, as the limited data precluded model learning and indicated inadequate nanopore sensitivity and capture ability toward the biomolecule. After excluding, the filtered dataset for each nanopore was split into a training set (80%) and a testing set (20%). A Random Forest classifier was chosen for its high classification accuracy. Model training and validation utilized 10-fold cross-validation. Corresponding cross-validation confusion matrices and learning curves are detailed in Fig. S12, S13, and S17.

The trained ML models were applied to predict labels for unlabeled events obtained from randomly mixed datasets, and experimentally measured mixtures. The mixture events were all underwent HDBSCAN pretreatment. Two fundamental assumptions are required to ensure the feasibility of relatively quantitative analysis: (1) The signal characteristics of each analyte within a given nanopore remain stable across single and mixed-component systems, with minimal interference, competitive effects, or shifts, thereby enabling accurate classification via machine learning even in complex mixtures. (2) All target analytes exhibit single-molecule translocation behavior, and their capture rates respond linearly to concentration changes within the tested range. Their translocation dynamics in mixed systems should remain comparable to those observed in pure conditions. Under these assumptions, a concentration-dependent model can be constructed based on the cross-validation strategy of multiple nanopores, enabling parallel relative quantitation across multiple types of biomolecules. For concentration prediction validation, simulated mixed datasets were constructed by randomly selecting events (within 3 min) based on the capture number statistics of pure analytes (Table S3). The classification process yielded the event count for each of the five analytes detected by each nanopore within the 3-minute data window as output data. To reduce prediction errors, each nanopore classified dataset was weighted according to its machine learning confusion matrix accuracy, enabling

nanopores with higher confidence to contribute more strongly to the fitting and thereby improving prediction accuracy and robustness. Here, the Pure Analyte Matrixes (*P*), Mixture Matrixes (*M*), and Accuracy Matrix (*A*) were constructed after machine learning. The *A* contains the cross-validation accuracy scores for each analyte classified as itself by each nanopore, serving as confidence weights (Fig. S12). The underlying relationship assumes that the mixture event counts result from the linear combination of the pure scaled by their respective unknown concentration coefficients is the fitted coefficient (α) calculated by (1):

$$N_M=\alpha\times N_P \quad (1)$$

where N_P represents the average event numbers per known concentration per analyte per nanopore (derived from pure sample data, Table S4), N_M contains the classified event counts per analyte per nanopore obtained from the mixture measurement or randomly generation within 3 min, α is the concentration coefficient of each analyte. The concentration coefficient vector was estimated by linear fitting algorithm using a weighted least squares (WLS) fitting approach. The *A* provided the weights, prioritizing predictions from nanopore-analyte combinations with higher classification accuracy during the minimization of residuals. After calculation, the α of each analyte can be predicted. The actual concentration of each analyte in a mixture is calculated by multiplying its concentration coefficient by its base concentration. The base concentrations are 2 μM WT EGFR ctDNA, 5 μM miR-21, 2 μM PD-L1 peptide, 1 mM DiLacNAc, and 2 μM FAD.

To maintain the accuracy of relative quantitative analysis, an upper concentration limit for the prediction algorithm was established. Using the average inter-event interval per unit concentration for each analyte (Table S8) as a reference, we defined the minimum resolvable detection interval as 10 ms. That is, only when the interval time between two successive events exceeds 10 ms can the system effectively resolve single-molecule translocation events. Based on this, the theoretical upper concentration detection limit for each analyte in isolation can be estimated by dividing the unit concentration inter-event time by 10 ms and multiplying the result by the current concentration as (2):

$$C_{upper}=[C]\times\frac{\tau_{on_{lowest}}}{10\ ms} \quad (2)$$

where C_{upper} is the highest concentration of each analyte, $[C]$ is the base concentration, the lowest of τ_{on} represents the lowest interval time of this analyte detected by four nanopores (Table S9).

On the other hand, analytes at very low concentrations face the risk of being obscured by background noise, making it difficult to reach the minimum threshold for reliable detection. To address this, we defined a theoretical lower concentration detection limit based on the twice events of background signals within a given time window. Thus the lower concentration of each analyte can be obtain by (3):

$$C_{lower}=[C]\times\frac{2\times N_{background}}{N_{analyte}} \quad (3)$$

where C_{lower} is the lower concentration of each analyte, the $N_{background}$ represents the capture events within 3 min of each nanopore and the $N_{analyte}$ represents each analyte detection with each nanopore. Choose the lower value form the equation as the final C_{lower} (Table S9). In practical applications, extending the recording time to enlarge the dataset further improves quantitative accuracy and lowers the detection limit.

All computational steps, including clustering, event feature extraction, machine learning, and discission-making were implemented in Python 3.10.16 using the Spyder development environment.

Supplementary Tables

Table S1 The sequence of biomolecules.

Analyte	Sequence[a]
Poly(dA)$_4$	5'-AAAA-3'
WT EGFR	5'-ATCAC-3'
T790M EGFR	5'-ATCAT-3'
miR-21	5'-UAGCUUAUC-3'
miR-92a	5'-UAUUGCAC-3'
PD-L1	LQDAGVYR
p-PD-L1	LQDAGVY$_P$R
DiLacNAc	Galβ1-4GlcNAcβ1-3Galβ1-4GlcNAc
LNT	Galβ1-3GlcNAcβ1-3Galβ1-4Glc
LNnT	Galβ1-4GlcNAcβ1-3Galβ1-4Glc

[a] Y_P: phosphotyrosine.

Table S2 The events per minute over three consecutive minutes.[a]

Analyte[b]	Nanopore	1 min	2 min	3 min
WT EGFR	KQ AeL	884	1023	913
PD-L1	TK/KQ AeL	645	600	643
FAD	TK/KQ AeL	1294	1377	1252
All	WT AeL	420	506	447
	KQ AeL	1105	994	1021
	TK/KQ AeL	1881	1819	1976
	WT OmpF	140	153	151

[a] Measurements for WT AeL, KQ AeL, and TK/KQ AeL were conducted at +100 mV, while WT OmpF was recorded at -100 mV. All data were recorded in 1.0 M KCl, 10 mM Tris, pH 8.0 with the sampling rate of 100 kHz and filtering at 5 kHz for 3 min on the 24-channel microchip using the homemade multichannel instrument.

[b] WT EGFR: 2 μM WT EGFR; PD-L1: 2 μM PD-L1; FAD: 2 μM FAD; All: 1 μM WT EGFR, 2.5 μM miR-21, 1 μM PD-L1 peptide, 0.5 mM DiLacNAc, and 1 μM FAD.

Table S3 Capture events and background signals of four nanopores.[a]

	EGFR	miR-21	PD-L1	DiLacNAc	FAD	Background
WT AeL	3320	1160	1060	270	2660	198
KQ AeL	2830	780	740	230	2970	421
TK/KQ AeL	3300	2240	1920	1630	3930	379
WT OmpF	0	0	290	260	0	23

[a] Capture events were obtained from the detection of 2 μM WT EGFR, 5 μM miR-21, 2 μM PD-L1, 1 mM DiLacNAc, and 2 μM FAD with four nanopores, respectively. The average capture-event counts were rounded to the nearest integer for subsequent simulated dataset construction, based on three independent experiments. Measurements for WT AeL, KQ AeL, and TK/KQ AeL were conducted at +100 mV, while WT OmpF was recorded at -100 mV within 3 min using 24-channel microchip.

Table S4 The pure analyte matrixes of identified events per known concentration per analyte per nanopore.[a]

		EGFR	miR-21	PD-L1	DiLacNAc	FAD
WT EGFR	WT AeL	129	14	0	0	25
	KQ AeL	1824	5	0	6	18
	TK/KQ AeL	2237	31	14	166	33
	WT OmpF	0	0	0	0	0
miR-21	WT AeL	2	161	2	0	18
	KQ AeL	0	196	0	95	20
	TK/KQ AeL	0	552	33	579	97
	WT OmpF	0	0	0	0	0
PD-L1	WT AeL	0	0	317	0	14
	KQ AeL	2	0	0	32	63
	TK/KQ AeL	0	103	478	165	103
	WT OmpF	0	0	46	27	0
DiLacNAc	WT AeL	0	0	0	0	0
	KQ AeL	0	0	0	70	12
	TK/KQ AeL	0	226	47	654	170
	WT OmpF	0	0	30	24	0
FAD	WT AeL	21	12	7	0	62
	KQ AeL	90	79	0	58	628
	TK/KQ AeL	10	194	81	308	1922
	WT OmpF	0	0	0	0	0

[a] The pure 2 µM WT EGFR, 5 µM miR-21, 2 µM PD-L1 peptide, 1 mM DiLacNAc, and 2 µM FAD were classified to each kind of molecule by machine learning models of four nanopores, respectively. Measurements for WT AeL, KQ AeL, and TK/KQ AeL were conducted at +100 mV, while WT OmpF was recorded at -100 mV within 3 min using 24-channel microchip.

Table S5 Classified events of a mixture sample containing of 2 μM WT EGFR and 2 μM PD-L1.[a]

	EGFR	miR-21	PD-L1	DiLacNAc	FAD
WT AeL	242	65	387	0	62
KQ AeL	1798	0	0	22	70
TK/KQ AeL	2839	81	397	189	84
WT OmpF	0	0	44	20	0

[a] Measurements for WT AeL, KQ AeL, and TK/KQ AeL were conducted at +100 mV, while WT OmpF was recorded at -100 mV within 3 min using 24-channel microchip.

Table S6 Classified events of a mixture sample containing of 2 μM WT EGFR, 2 μM PD-L1, and 2 μM FAD.[a]

	EGFR	miR-21	PD-L1	DiLacNAc	FAD
WT AeL	194	70	367	0	129
KQ AeL	1415	52	0	66	464
TK/KQ AeL	3036	209	559	417	2898
WT OmpF	0	0	51	20	0

[a] Measurements for WT AeL, KQ AeL, and TK/KQ AeL were conducted at +100 mV, while WT OmpF was recorded at -100 mV within 3 min using 24-channel microchip.

Table S7 Classified events of a mixture sample containing of 1 µM WT EGFR, 2.5 µM miR-21, 1 µM PD-L1 peptide, 0.5 mM DiLacNAc, and 1 µM FAD.[a]

	EGFR	miR-21	PD-L1	DiLacNAc	FAD
WT AeL	5	0	33	0	40
KQ AeL	655	90	0	129	222
TK/KQ AeL	991	820	449	738	1398
WT OmpF	0	0	58	42	0

[a] Measurements for WT AeL, KQ AeL, and TK/KQ AeL were conducted at +100 mV, while WT OmpF was recorded at -100 mV within 3 min using 24-channel microchip.

Table S8 The statistical interval time (τ_{on}) of five biomolecules detected with four nanopores respectively.[a]

	EGFR / ms	miR-21 / ms	PD-L1 / ms	DiLacNAc / ms	FAD / ms
WT AeL	963.5	800.1	453.3	2068.0	324.2
KQ AeL	76.0	580.4	712.1	1464.6	326.0
TK/KQ AeL	48.2	143.8	343.4	111.9	96.8
WT OmpF[b]	-	-	1576.6	3054.1	-

[a] Measurements for WT AeL, KQ AeL, and TK/KQ AeL were conducted at +100 mV, while WT OmpF was recorded at -100 mV using 24-channel microchip.

[b] -: Due to the low capture frequency, WT EGFR, miR-21, and FAD were rarely observed in WT OmpF, and thus the interval time could not be calculated.

Table S9 The upper detection limit and lower detection limit of concentration of each pure biomolecule for effective quantification.

	Upper detection limit / μM	Lower detection limit / μM
EGFR	9.6	0.2
miR-21	71.9	1.7
PD-L1	68.7	0.3
DiLacNAc	11190.0	176.9
FAD	19.4	0.3

Supplementary Figures

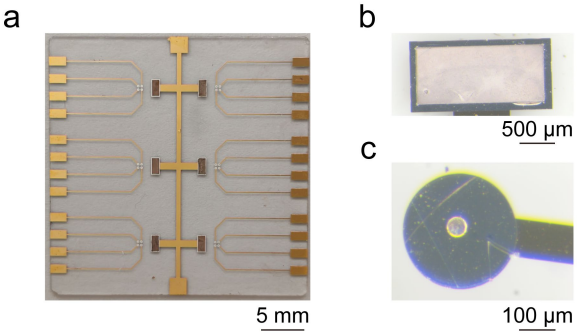

Fig. S1 The optical images of the low noise bioelectronic microchip. (a) The image of the 24-channel microchip. (b) The image of an Ag/$AgCl_{cis}$ as a ground electrode. (c) The image of an Ag/$AgCl_{trans}$ microelectrode to apply voltage.

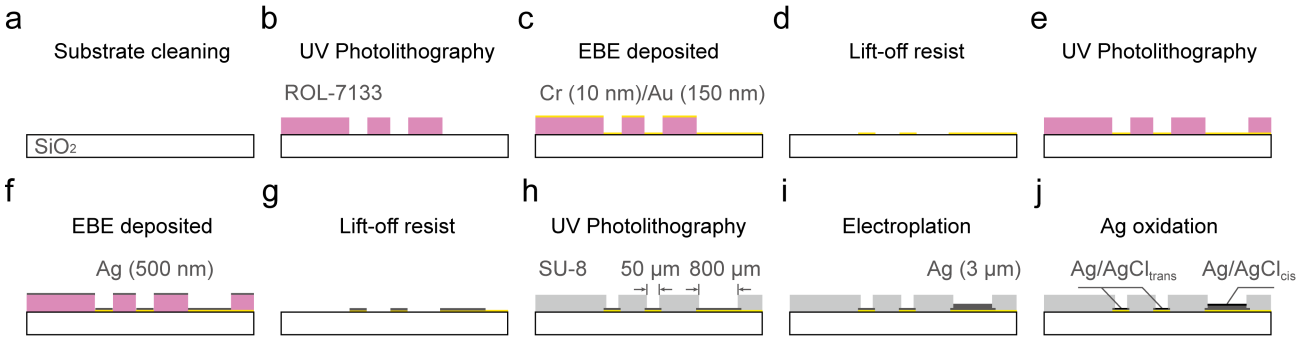

Fig. S2 Fabrication process of the microchip. (a) The substrate was cleaned with ultrapure water and isopropanol, dried under N_2, and baked on a 120 °C hotplate for 10 min. (b) A negative photoresist (ROL-7133) was spin-coated and patterned by UV photolithography. (c) A Cr (10 nm) adhesion layer and an Au (150 nm) conductive layer were sequentially deposited by electron-beam evaporation (EBE). (d) Lift-off was performed to define the wiring area. (e) ROL-7133 layer was spin-coated again and patterned by UV exposure. (f) A 500 nm Ag layer was deposited by EBE. (g) Lift-off was carried out to define the electrode area. (h) An SU-8 layer was patterned by UV photolithography to form an array of 50 μm-diameter microwells and microelectrodes, along with ground electrodes. (i) A ~3 μm-thick Ag layer was electroplated to form the $Ag/AgCl_{cis}$ electrode. (j) The Ag surface was oxidized in NaClO solution to produce the Ag/AgCl electrode. The schematic illustrates two representative microwells ($Ag/AgCl_{trans}$ electrode) and one $Ag/AgCl_{cis}$ electrode integrated within a shared chamber. Not to scale.

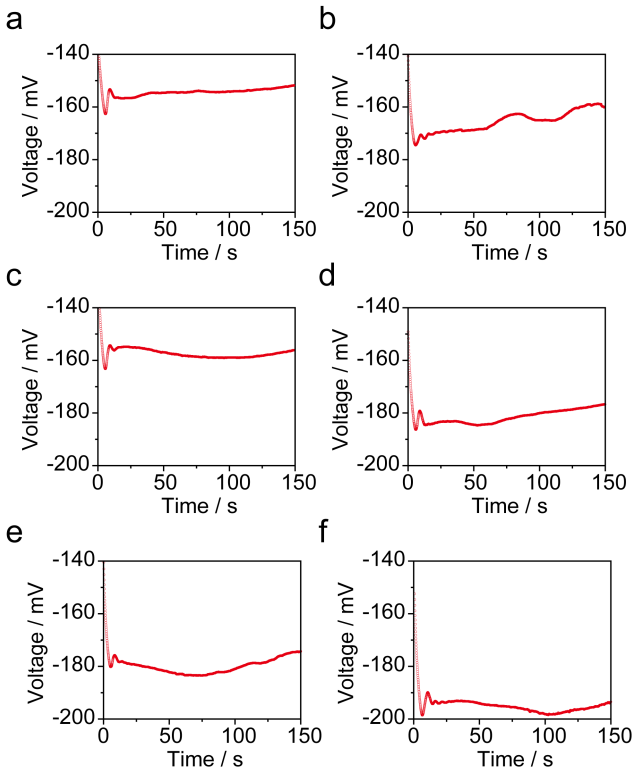

Fig. S3 Electrochemical Ag plating using chronopotentiometry. (a-f) Voltage-time curves recorded during Ag electroplating of chambers one to six. The Ag layer was deposited from 0.3 M $AgNO_3$ in 1 M $NH_3{\cdot}H_2O$ using a three-electrode cell with the patterned Ag on the microchip as the working electrode, an Ag wire as the quasi-reference electrode, and a Pt wire as the counter electrode. The plating was carried out at room temperature under a constant current density of 0.33 mA/mm² (475 µA per pattern) for 150 s, yielding a ~3 µm Ag layer to improve the stability of $Ag/AgCl_{cis}$ electrode. A minor voltage bias mainly originates from inter-channel heterogeneity, which could be corrected via software-based voltage compensation before single-channel recording to maintaining stable and uniform electrode potentials.

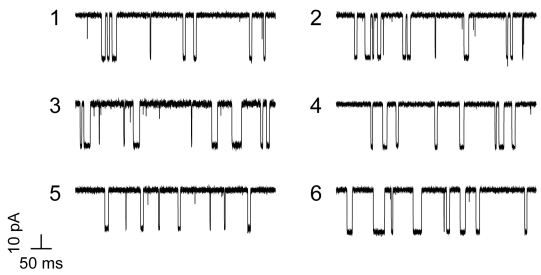

Fig. S4 Current traces of Poly(dA)$_4$ detection with WT AeL nanopores in chambers one to six. Membrane arrays were formed by a manual air bubble method on a single 24-channel microchip. One representative channel from each chamber is shown to demonstrate the consistency across the microchip. All data were recorded in 1.0 M KCl, 10 mM Tris, pH 8.0 at +100 mV with a sampling rate of 100 kHz and a 5 kHz low-pass filter.

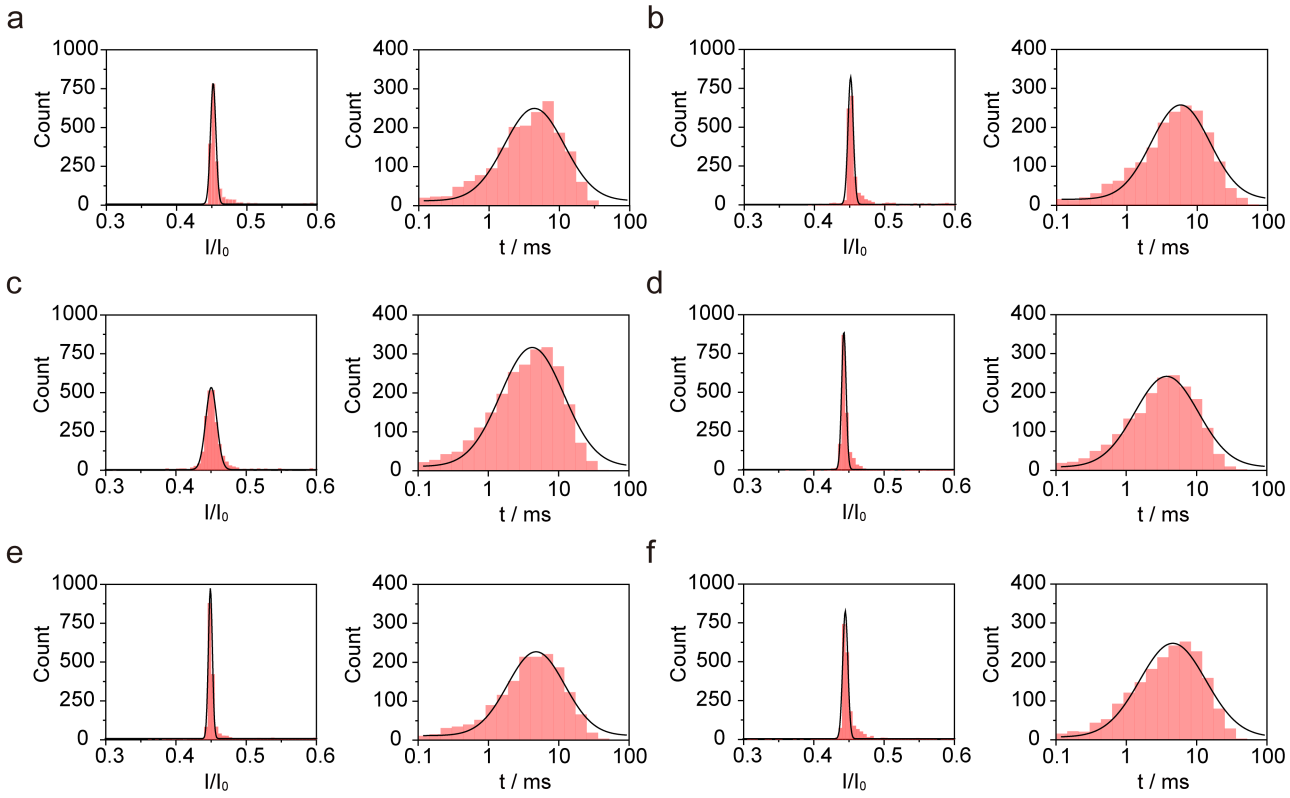

Fig. S5 Statistical analysis of Poly(dA)$_4$ detection with WT AeL on the 24-channel microchip. (a-f) Statistical histograms (red columns) and Gaussian fittings (black lines) of I/I_0 (left) and the single exponential fittings of duration time (t, right) for Poly(dA)$_4$ in chambers one to six. One representative channel was selected from each four-channel chamber to demonstrate the consistency across the microchip. All data were recorded in 1.0 M KCl, 10 mM Tris, pH 8.0 at +100 mV, with a sampling rate of 100 kHz, low-pass filtered at 5 kHz, and analyzed using 3000 events.

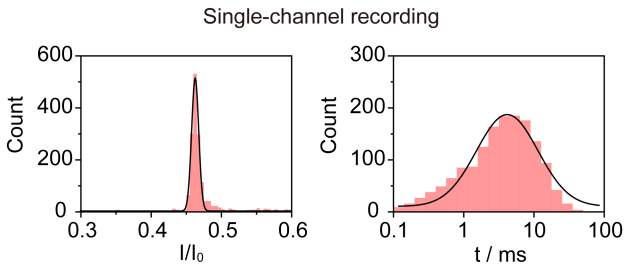

Fig. S6 Poly(dA)$_4$ detection with WT AeL on the single-channel platform. Statistical histograms (red columns) and Gaussian fittings (black lines) of I/I_0 (0.46, left) and the single exponential fitting of t (4.2 ms, right) using a single-channel recording platform. Single-channel measurements were conducted using the homemade Cube-D0 instrument and a thin-film chamber with a 50 μm aperture, shown an open-pore current STD of 1.6 ± 0.3 pA. These experiments confirmed that the single-channel translocation events were basically consistent with those observed in the 24-channel microchip system (Fig. S5). All data were recorded in 1.0 M KCl, 10 mM Tris, pH 8.0 at +100 mV, with a sampling rate of 100 kHz, low-pass filtered at 5 kHz with 2000 events.

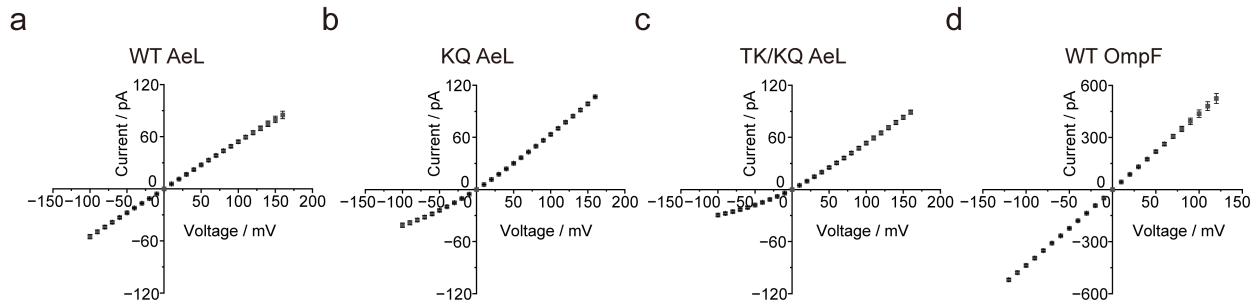

Fig. S7 I-V curves of various nanopores measured on the 24-channel microchip. I-V curves of (a) WT AeL, (b) KQ AeL, (c) TK/KQ AeL, and (d) WT OmpF nanopore. Error bars represent data from three independent nanopores. The I-V characteristics recorded on the microchip were consistent with those from the single-channel platform, confirming that the multichannel system provides reliable, reproducible, and stable performance. All data were recorded in 1.0 M KCl, 10 mM Tris, pH 8.0, with a sampling rate of 100 kHz, low-pass filtered at 5 kHz.

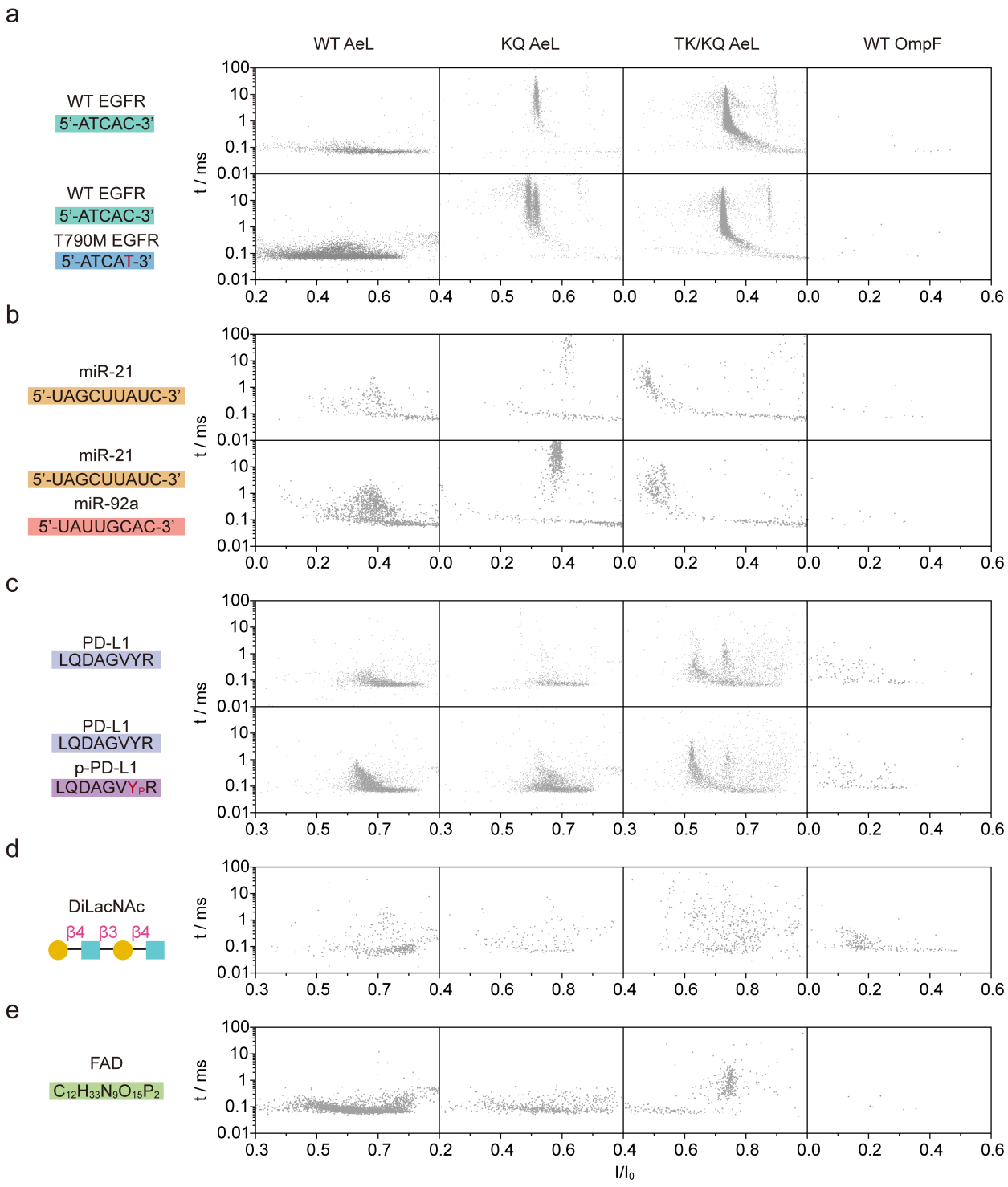

Fig. S8 Multiple biomolecules detection with various nanopores on a single-channel platform. (a) Detection of WT EGFR ctDNA and its mixture with T790M EGFR using WT AeL, KQ AeL and TK/KQ AeL at +140 mV, and WT OmpF at -100 mV respectively (from left to right). (b) Detection of miR-21 and its mixture with miR-92a in DEPC-treated water using WT AeL, KQ AeL and TK/KQ AeL at +100 mV, and WT OmpF at -100 mV respectively (from left to right). (c) Detection of PD-L1 peptide and its mixture with p-PD-L1 using WT AeL, KQ AeL and TK/KQ AeL at +140 mV, and WT OmpF at -100 mV respectively (from left to right). (d) Detection of DiLacNAc using WT AeL, KQ AeL and TK/KQ AeL at +100 mV, and WT OmpF at -100 mV respectively (from left to right). (e) Detection of FAD using WT AeL, KQ AeL and TK/KQ AeL at +80 mV, and WT OmpF at -100 mV respectively (from left to right). As a result, the WT AeL gives responses to ctDNA, miRNA, peptide fragments and small-molecule metabolites. The KQ AeL could detect ctDNA, miRNA, and FAD, exhibiting the highest

discrimination ability for WT EGFR and its single-nucleotide mutant T790M. The TK/KQ AeL nanopore can effectively differentiate miR-21 and miR-92a fragments, peptide fragment from PD-L1 with or without tyrosine phosphorylation, as well as small metabolic molecules such as FAD. While TK/KQ AeL was able to detect EGFR ctDNA (the scatter peak with fewer events may result from impurities or sample degradation), it struggle to distinguish EGFR framents differing by a single nucleotide. The WT OmpF reliably detects PD-L1 and oligosaccharides, but has minimal response to other biomolecules. All data were recorded in 1.0 M KCl, 10 mM Tris, pH 8.0, sampled at 100 kHz and low-pass filtered at 5 kHz for 3 min, using the homemade Cube-D0 instrument and a thin-film chamber with a 50 μm aperture.

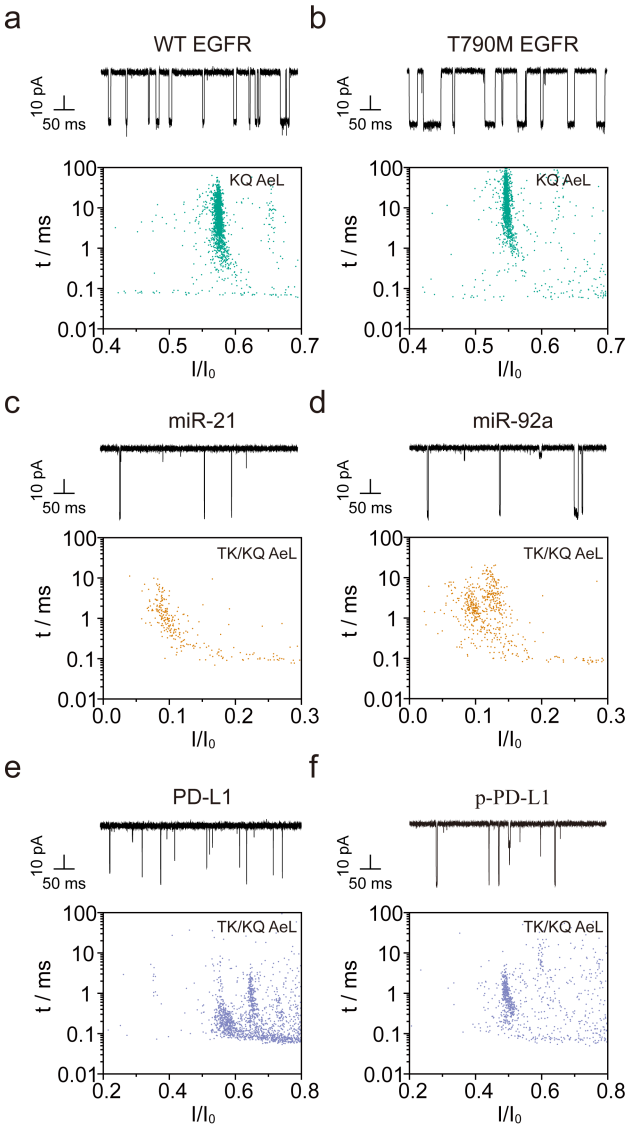

Fig. S9 Detection of pure biomolecules with various nanopores on the 24-channel microchip. (a) Detection of 2 μM EGFR ctDNA with KQ AeL at +140 mV. (b) Detection of 2 μM T790M ctDNA with KQ AeL at +140 mV. (c) Detection of 5 μM miR-21 with TK/KQ AeL at +100 mV. (d) Detection of 5 μM miR-92a with TK/KQ AeL at +100 mV. (e) Detection of 2 μM PD-L1 peptide with TK/KQ AeL at +140 mV. (f) Detection of 2 μM p-PD-L1 with TK/KQ AeL at +140 mV. When detecting miR-21 and miR-92a, DEPC-treated water was used as the solvent to minimize RNA degradation. All data were recorded in 1.0 M KCl, 10 mM Tris, pH 8.0 with the sampling rate of 100 kHz and filtering at 5 kHz, using the homemade multichannel instrument.

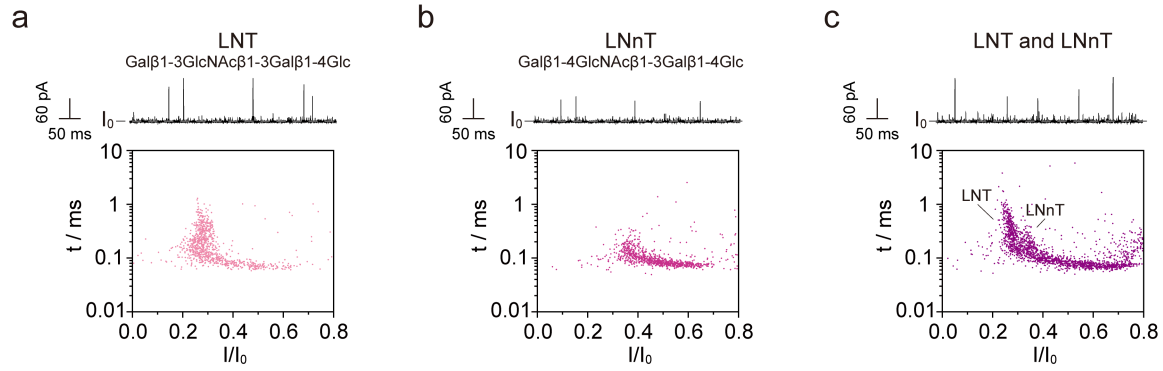

Fig. S10 The oligosaccharides detection with WT OmpF nanopore on the 24-channel microchip. The (a) 500 µM LNT detection with 1000 events, (b) 500 µM LNnT detection with 1000 events, and (c) their mixture detection with 2000 events detection by WT OmpF at the applied voltage of -120 mV. The LNT and LNnT tetrasaccharides constitute the essential components of human milk oligosaccharides (HMOs) playing versatile physiological functions,[11] which can be identified using WT OmpF nanopore. All data were recorded in 1.0 M KCl, 10 mM Tris, pH 8.0 with the sampling rate of 100 kHz and filtering at 5 kHz, using the homemade multichannel instrument.

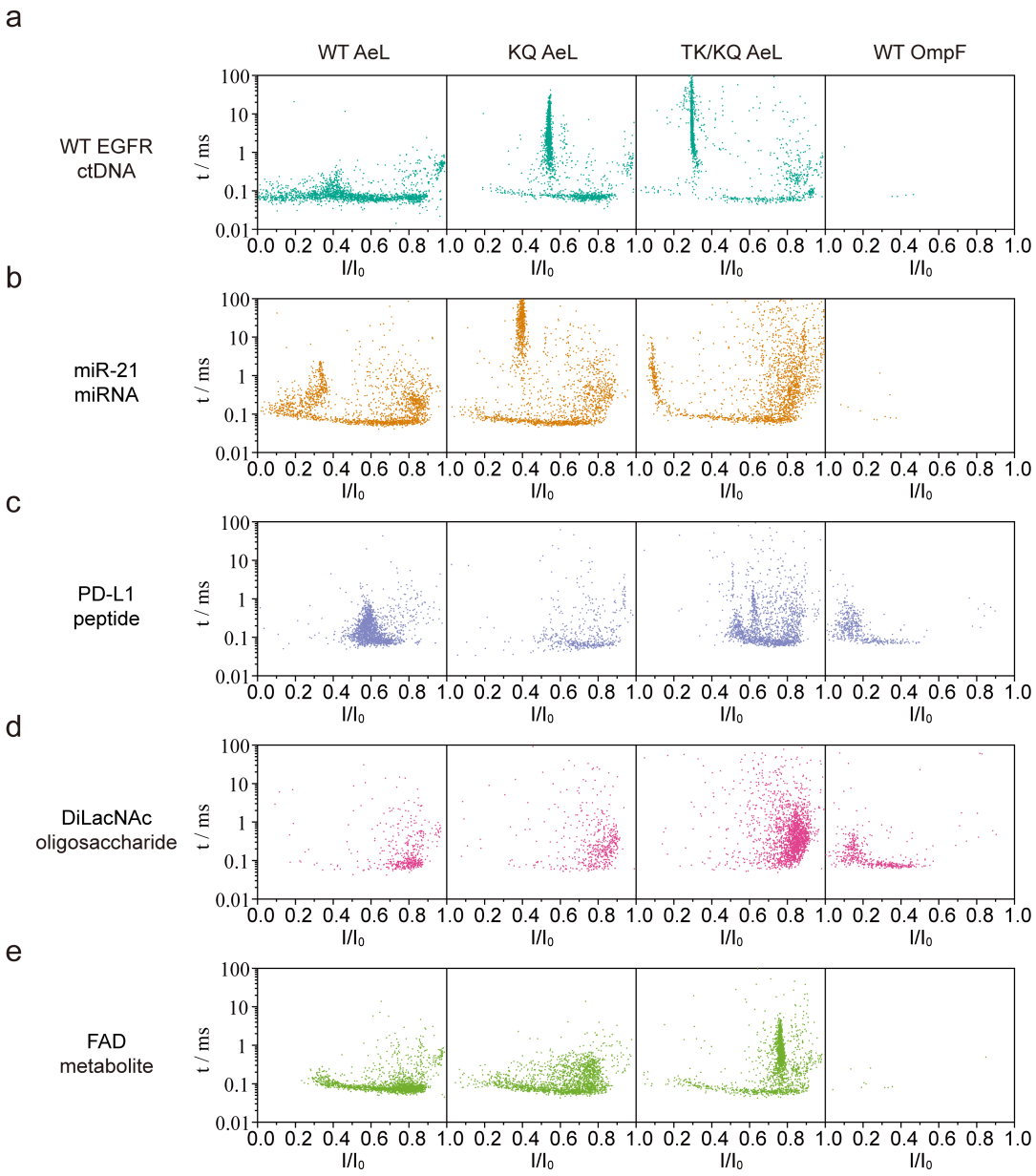

Fig. S11 Multiple biomolecules detection with various nanopores on the 24-channel microchip. (a) Detection of 2 μM WT EGFR ctDNA by WT AeL with 2000 events, KQ AeL with 2000 events and TK/KQ AeL with 2000 events at +100 mV, as well as WT OmpF with 5 events at -100 mV respectively (from left to right). (b) Detection of 5 μM miR-21 by WT AeL with 2000 events, KQ AeL with 2000 events and TK/KQ AeL with 2000 events at +100 mV, as well as WT OmpF with 10 events at -100 mV respectively (from left to right). (c) Detection of 2 μM PD-L1 peptide by WT AeL with 2000 events, KQ AeL with 500 events and TK/KQ AeL with 2000 events at +100 mV, as well as WT OmpF with 500 events at -100 mV respectively (from left to right). (d) Detection of 1 mM DiLacNAc by WT AeL with 500 events, KQ AeL with 500 events and TK/KQ AeL with 2000 events at +100 mV, as well as WT OmpF with 500 events at -100 mV respectively (from left to right). (e) Detection of 2 μM FAD by WT AeL with 2000 events, KQ AeL with 2000 events and TK/KQ AeL with 2000 events at +100 mV, as well as WT OmpF with 10 events at -100 mV respectively (from left to right). The statistical results were comparable with those from the single-channel platform, showing reproducible features for various biomarkers sensing. The bias of events number was from the diverse capture capabilities of nanopores for each biomolecule. When detecting miR-21, DEPC-treated water was used as the solvent to minimize RNA degradation. All data were recorded in 1.0 M KCl, 10 mM Tris, pH 8.0 with the sampling rate of 100 kHz and filtering at 5 kHz using the homemade multichannel instrument.

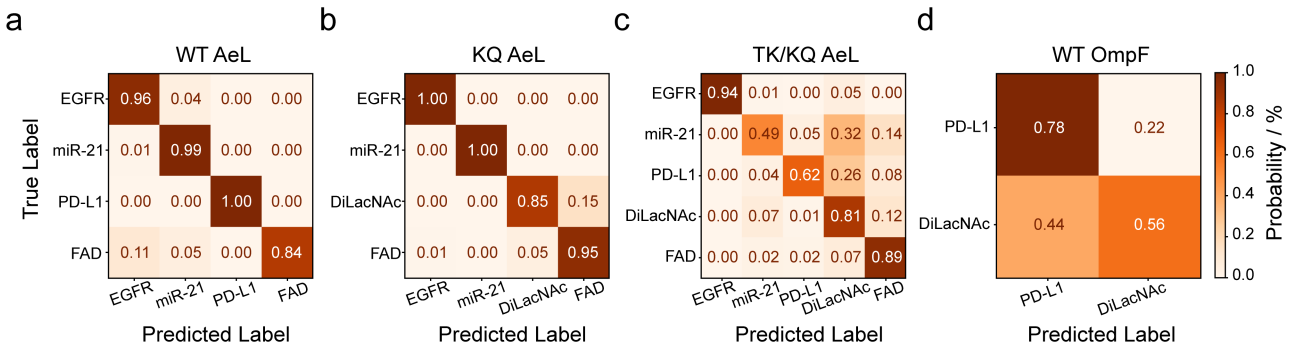

Fig. S12 Cross-validation confusion matrixes for the machine learning (ML) classification models. The cross-validation confusion matrixes of (a) WT AeL, (b) KQ AeL, (c) TK/KQ AeL, and (d) WT OmpF for various biomolecules. The datasets of WT EGFR, miR-21, PD-L1, DiLacNAc, and FAD detection with WT AeL, KQ AeL, TK/KQ AeL, and WT OmpF respectively were input into Random Forest based Machine Learning model for biomolecules identification. Analytes yielding fewer than 10 events after Hierarchical Density-Based Spatial Clustering of Applications with Noise (HDBSCAN) denoising were treated as unclassifiable, as the limited data prevented model learning and indicated insufficient sensitivity and capture ability. Thus, WT AeL could identify WT EGFR, miR-21, PD-L1, and FAD; KQ AeL could classify WT EGFR, miR-21, DiLacNAc, and FAD; TK/KQ Ael was capable of identifying all five biomolecules; whereas WT OmpF could only classify PD-L1 and DiLacNAc. All data were recorded in 1.0 M KCl, 10 mM Tris, pH 8.0 with the sampling rate of 100 kHz and filtering at 5 kHz on the 24-channel microchip using the homemade multichannel instrument.

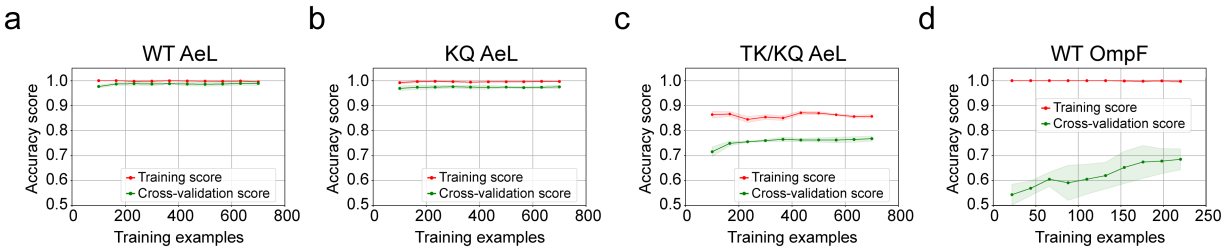

Fig. S13 Learning curves for the ML classification models. The learning curves of (a) WT AeL, (b) KQ AeL, (c) TK/KQ AeL, and (d) WT OmpF for various biomolecules. Notably, because that WT OmpF could only detect PD-L1 and DiLacNAc, its training examples in the learning curve were only 220 events available.

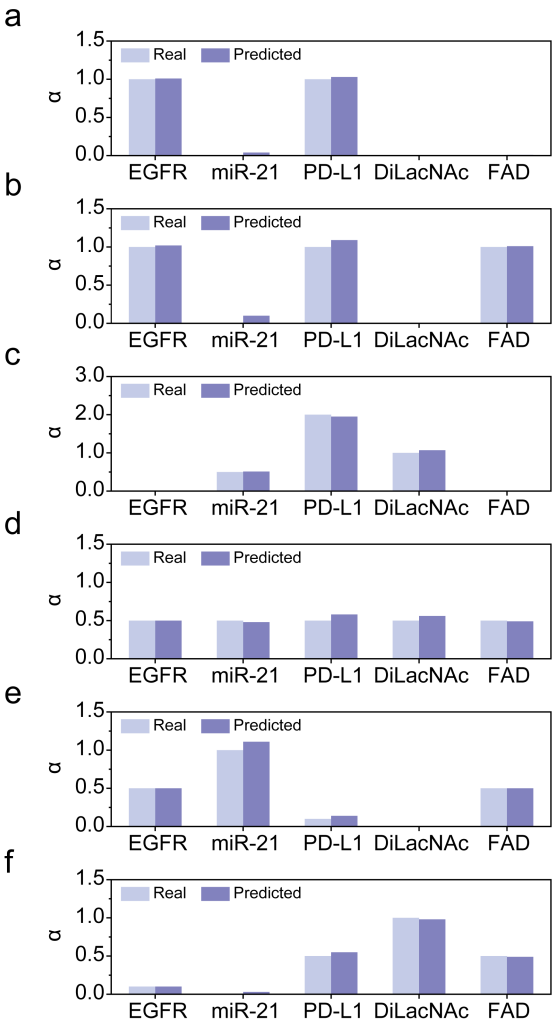

Fig. S14 Concentration prediction of mixed simulated datasets. Simulated mixture datasets were generated by randomly sampling events from pure analyte datasets according to their respective 3-min capture frequencies (Table S3), simulating mixtures of various analyte proportions. Each mixture was designed with predefined concentration coefficients (α) for the five analytes (WT EGFR : miR-21 : PD-L1 : DiLacNAc : FAD): (a) 1 : 0 : 1 : 0 : 0; (b) 1 : 0 : 1 : 0 : 1; (c) 0 : 0.5 : 2 : 1 : 0; (d) 0.5 : 0.5 : 0.5 : 0.5 : 0.5; (e) 0.5 : 1 : 0.1 : 0 : 0.5; (f) 0.1 : 0 : 0.5 : 1 : 0.5. The predicted α values represent the relative concentration coefficients of each analyte, where the predicted concentration is given by α multiplied by its base (pure) concentration. Each mixture was classified using the machine-learning models trained on WT AeL, KQ AeL, TK/KQ AeL, and WT OmpF nanopores, respectively. The light-purple bars indicate the theoretical α expected from the predefined synthetic ratios, while the dark-purple bars show the predicted α obtained from the multiple nanopore cross-validation based linear fitting algorithm using a weighted least squares approach. The base concentrations were 2 μM WT EGFR ctDNA segment, 5 μM miR-21 segment, 2 μM PD-L1 peptide, 1 mM DiLacNAc, and 2 μM FAD. All data were recorded in 1.0 M KCl, 10 mM Tris, pH 8.0 for 3 min with the sampling rate of 100 kHz and filtering at 5 kHz on the 24-channel microchip using the homemade multichannel instrument.

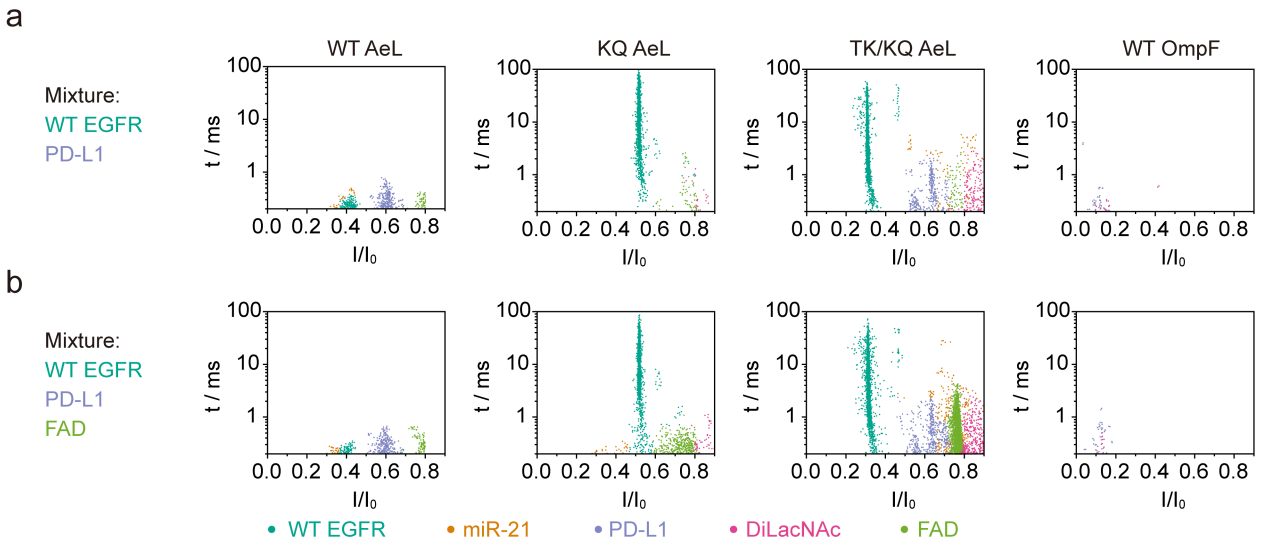

Fig. S15 Scatter plots of mixture samples classified by ML models on the 24-channel microchip. (a) Scatter plots of a mixture containing 2 µM WT EGFR and 2 µM PD-L1 detected with WT AeL, KQ AeL and TK/KQ AeL at +100 mV, and WT OmpF at -100 mV, respectively (from left to right). (b) Scatter plots of a mixture containing 2 µM WT EGFR, 2 µM PD-L1, and 2 µM FAD detected with WT AeL, KQ AeL and TK/KQ AeL at +100 mV, and WT OmpF at -100 mV respectively (from left to right). In each plot, the x-axis denotes the I/I_0 (0.0-0.9), and the y-axis denotes the events duration time (0.2-100 ms). The colored events represent molecular types predicted by the ML model trained on WT AeL, KQ AeL, TK/KQ AeL, and WT OmpF, respectively. All data were recorded in 1.0 M KCl, 10 mM Tris, pH 8.0 with the sampling rate of 100 kHz and filtering at 5 kHz for 3 min using the homemade multichannel instrument.

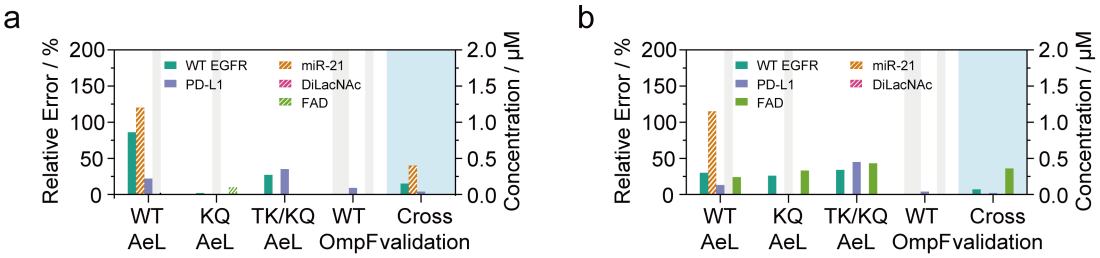

Fig. S16 Concentration prediction relative error and the predicted values. The predicted concentration of mixtures containing (a) 2 μM EGFR and 2 μM PD-L1, and (b) 2 μM EGFR, 2 μM PD-L1 and 2 μM FAD as calculated by WT AeL, KQ AeL, TK/KQ AeL, WT OmpF, and the cross-validation of all four nanopores. The left y-axis and the solid color bars (without diagonal lines) represent the relative prediction error compared with the true concentration. Relative error is defined as the absolute difference between the predicted and true values, divided by the true value. The right y-axis and the bars with white diagonal lines represent the predicted concentration of analytes absent in the mixture. Gray bars indicate analytes that cannot be sensed by the corresponding nanopore, as determined by the machine learning model (Fig. S12). Blue bars highlight the lowest error achieved by the multi-nanopore cross-validation method for five types of biomolecules. The applied voltages were +100 mV for WT AeL, KQ AeL, and TK/KQ AeL, and -100 mV for WT OmpF. All data were recorded in 1.0 M KCl, 10 mM Tris, pH 8.0 with the sampling rate of 100 kHz and filtering at 5 kHz for 3 min on the 24-channel microchip using the homemade multichannel instrument.

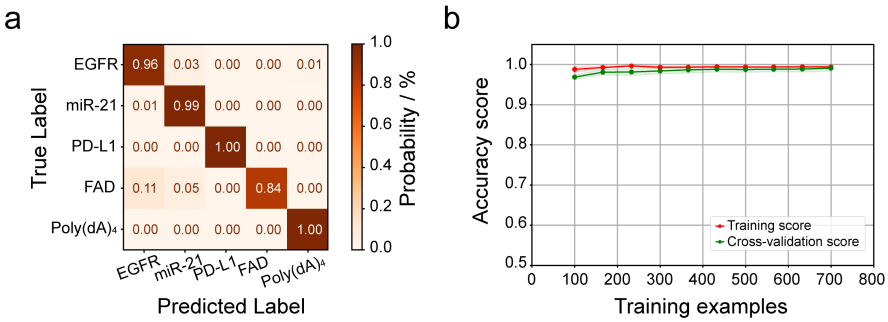

Fig. S17 Multiple biomolecules classification with WT AeL using machine learning model. The (a) cross-validation confusion matrix and (b) learning curve of Poly(dA)$_4$, WT EGFR, miR-21, PD-L1, DiLacNAc, and FAD, detected with WT AeL. All data were recorded in 1.0 M KCl and 10 mM Tris, pH 8.0 at +100 mV with the sampling rate of 100 kHz and filtering at 5 kHz on the 24-channel microchip using the homemade multichannel instrument.

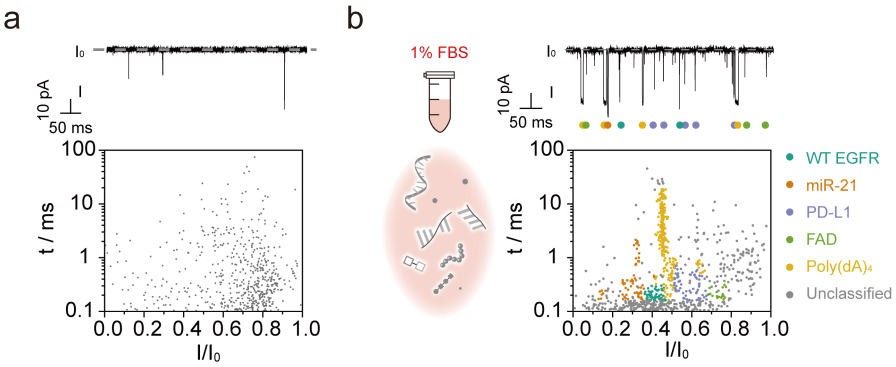

Fig. S18 Detection of mixture samples by WT AeL in FBS. (a) The current trace and background signals of WT AeL within 1% FBS for 3 min. (b) Current trace and scatter plot of a mixture containing 2 µM Poly(dA)$_4$, 2 µM EGFR, 5 µM miR-21, 2 µM PD-L1, 1 mM DiLacNAc, and 2 µM FAD in 1% FBS for 1 min. The colored events represent molecular types predicted by the ML model trained on WT AeL, whereas the gray events correspond to noise-filtered points removed by HDBSCAN. The Poly(dA)$_4$ was used for microchip and nanopore calibration. All data were recorded in 1.0 M KCl, 10 mM Tris, pH 8.0, prepared in DEPC-treated water at +100 mV with the sampling rate of 100 kHz and filtering at 5 kHz on the 24-channel microchip using the homemade multichannel instrument.

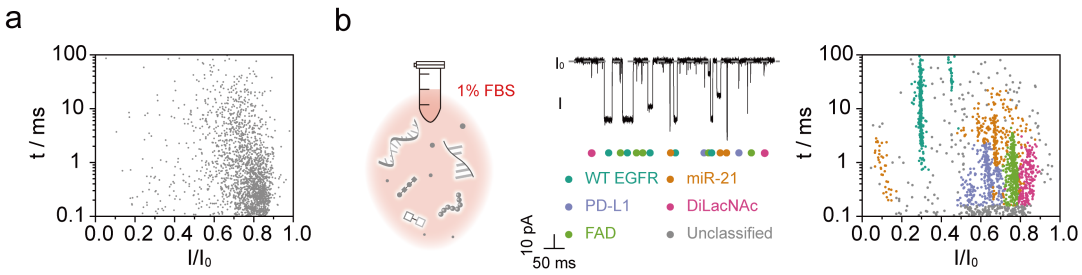

Fig. S19 Detection of complex samples by TK/KQ AeL in FBS. (a) Scatter plot of the background signal of TK/KQ AeL in 1% FBS without analytes for 3 min. (b) Current trace and scatter plot of a mixture containing 2 µM WT EGFR, 5 µM miR-21, 2 µM PD-L1, 1 mM DiLacNAc, and 2 µM FAD in 1% FBS for 1 min. The colored events represent molecular types predicted by the ML model trained on TK/KQ AeL, whereas the gray events correspond to noise-filtered points removed by HDBSCAN. All data were recorded in 1.0 M KCl and 10 mM Tris, pH 8.0, prepared in DEPC-treated water at +100 mV with the sampling rate of 100 kHz and filtering at 5 kHz on the 24-channel microchip using the homemade multichannel instrument.

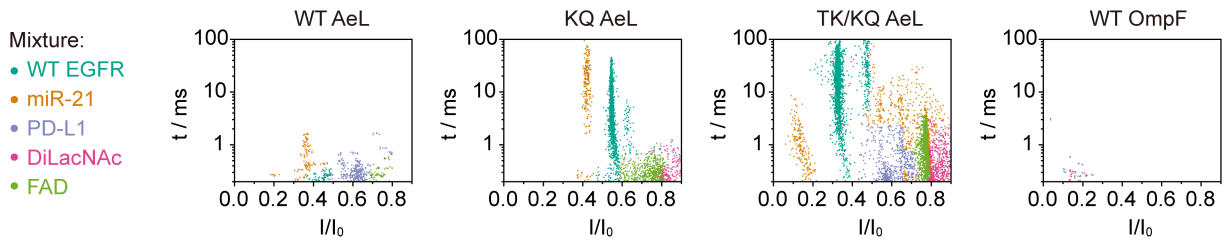

Fig. S20 Scatter plots of the mixture containing five types of biomolecules classified by ML models on the 24-channel microchip. Scatter plots of a mixture containing 2 μM WT EGFR ctDNA, 5 μM miR-21, 2 μM PD-L1 peptide, 1 mM DiLacNAc, and 2 μM FAD, detected with WT AeL, KQ AeL and TK/KQ AeL at +100 mV, and WT OmpF at -100 mV respectively (from left to right). In each plot, the x-axis denotes the I/I_0 (0.0-0.9), and the y-axis denotes the duration time (0.2-100 ms). The colored events represent molecular types predicted by the ML model trained on WT AeL, KQ AeL, TK/KQ AeL, and WT OmpF, respectively. All data were recorded in 1.0 M KCl, 10 mM Tris, pH 8.0, prepared in DEPC-treated water with the sampling rate of 100 kHz and filtering at 5 kHz on the 24-channel microchip using the homemade multichannel instrument.

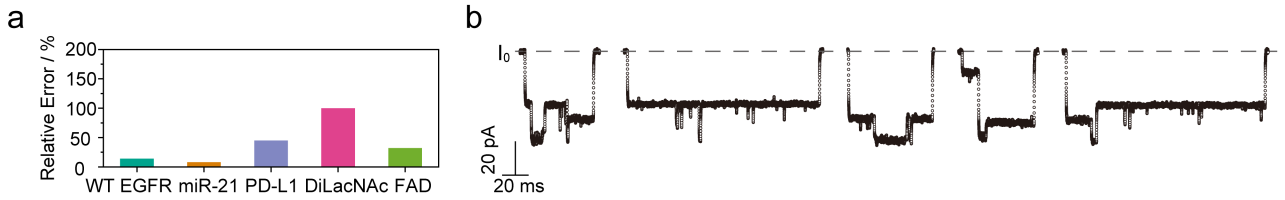

Fig. S21 Concentration prediction relative error and typical multicomponent translocation events for a mixture containing five biomolecules**.** (a) Relative error of concentration predictions for a mixture containing 2 μM WT EGFR, 5 μM miR-21, 2 μM PD-L1 peptide, 1 mM DiLacNAc, and 2 μM FAD detected with WT AeL, KQ AeL and TK/KQ AeL at +100 mV, and WT OmpF at -100 mV, respectively. (b) Representative ionic current traces showing simultaneous translocation events of multiple biomolecules through TK/KQ AeL. At high analyte concentrations, prevalent co-translocation events[12] hinder accurate signal identification and event counting, leading to substantial discrepancies between the predicted and actual concentrations. All data were recorded in 1.0 M KCl and 10 mM Tris, pH 8.0, prepared in DEPC-treated water, at a sampling rate of 100 kHz and low-pass filtered at 5 kHz, using a 24-channel microchip and a homemade multichannel instrument.

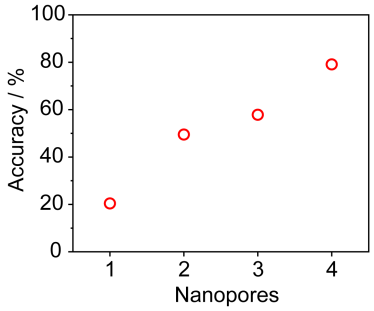

Fig. S22 Concentration prediction accuracy obtained using different numbers of nanopores. The data were obtained from a mixture containing 1 µM WT EGFR ctDNA, 2.5 µM miR-21, 1 µM PD-L1 peptide, 0.5 mM DiLacNAc, and 1 µM FAD, detected with WT AeL, KQ AeL and TK/KQ AeL at +100 mV, and with WT OmpF at -100 mV, respectively. From one to four nanopores, the model first used WT OmpF, which could predict only PD-L1 and DiLacNAc due to its molecular selectivity; then incorporated TK/KQ AeL for five-biomolecule prediction; next added WT AeL; and finally introduced KQ AeL. The accuracy was defined as 100% minus the average relative error, where the average relative error represents the mean relative error of the biomolecules that could be predicted within each nanopore combination. The relative error was calculated as the absolute difference between the predicted and true values divided by the true value. As the number of nanopores increased from one to four, the prediction accuracy improved progressively, suggesting that incorporating additional nanopores may allow the accuracy to approach nearly 100%. All data were recorded in 1.0 M KCl, 10 mM Tris, pH 8.0 with the sampling rate of 100 kHz and filtering at 5 kHz on the 24-channel microchip using the homemade multichannel instrument.

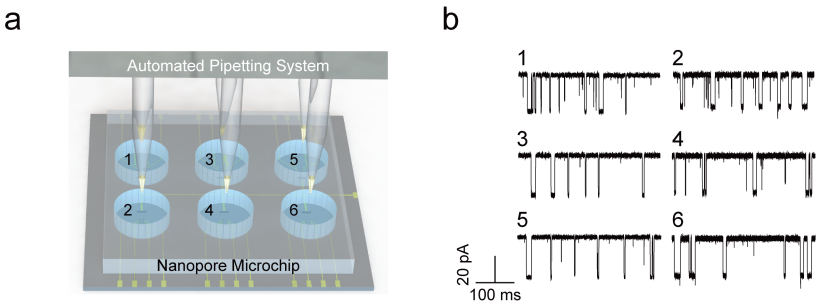

Fig. S23 The automatic nanopore microchip operated by automated multi-channel liquid handling system. (a) The scheme of the platform. (b) The current traces of Poly(dA)$_4$ detection by WT AeL from chamber one to six using automated multi-channel liquid handling system on the 24-channel microchip. The All data were recorded at the applied voltage of +100 mV with the sampling rate of 100 kHz and filtering at 5 kHz on the microchip using the homemade multichannel instrument.

References

1 F. Gao, J. H. Wang, H. Ma, B. Xia, L. Wen, Y. T. Long and Y. L. Ying, *Angew. Chem. Int. Ed.*, 2025, **64**, e202422118.

2 L.-L. Zhang, C.-B. Zhong, T.-J. Huang, L.-M. Zhang, F. Yan and Y.-L. Ying, *Chem. Sci.*, 2024, **15**, 8355-8362.

3 J. Wang, S.-C. Liu, Z.-L. Hu, Y.-L. Ying and Y.-T. Long, *J. Am. Chem. Soc.*, 2025, **147**, 1781-1791.

4 Y.-H. Fu, X. Li, L. Ma, Y.-J. Wan, L.-M. Zhang, Y.-L. Ying and Y.-T. Long, *J. Phys. Chem. C*, 2024, **128**, 1110-1115.

5 M.-Y. Li, Y.-Q. Wang, Y.-L. Ying and Y.-T. Long, *Chem. Sci.*, 2019, **10**, 10400.

6 L.-L. Zhang, C.-B. Zhong, J.-G. Li, H.-Y. Niu, Y.-L. Ying and Y.-T. Long, *J. Electroanal. Chem.*, 2022, **915**, 116266.

7 Z.-L. Hu, Y.-L. Ying, M.-Z. Huo, X.-F. Kong, X.-D. Yu, J.-R. Zhang and Y.-T. Long, *J. Chem. Educ.*, 2020, **97**, 4345-4354.

8 A. Balijepalli, J. Ettedgui, A. T. Cornio, J. W. F. Robertson, K. P. Cheung, J. J. Kasianowicz and C. Vaz, *ACS Nano*, 2014, **8**, 1547.

9 J. Jiang, M.-Y. Li, X.-Y. Wu, Y.-L. Ying, H.-X. Han and Y.-T. Long, *Nat. Chem.*, 2023, **15**, 578-586.

10 G. Yao, B. Xia, F. Wei, J. Wang, Y. Yang, S. Ma, W. Ke, T. Li, X. Cheng, L. Wen, Y.-T. Long and Z. Gao, *J. Am. Chem. Soc.*, 2025, **147**, 1721-1731.

11 Y. Zhu, G. Luo, L. Wan, J. Meng, S. Y. Lee and W. Mu, *Crit. Rev. Biotechnol.*, 2021, **42**, 578.

12 C. Plesa, D. Verschueren, S. Pud, J. van der Torre, J. W. Ruitenberg, M. J. Witteveen, M. P. Jonsson, A. Y. Grosberg, Y. Rabin and C. Dekker, *Nat. Nanotechnol.*, 2016, **11**, 1093-1097.